Removal of Hg (II) from synthetic and real water using green iron oxide nanoparticles: Equilibrium, kinetic and thermodynamic studies.

Wilfredo Marimón-Bolívar[a], Lesly Tejeda-Benitez[b].

a. Research Group in Engineering for Sustainability - GRIIS, Department of Civil Engineering, Universidad Catolica de Colombia.

b. Facultad de Ingeniería, Universidad de Cartagena, Cartagena, Colombia

ABSTRACT

New environmentally friendly routes are being investigated to obtain nanomaterials that can be implemented in environmental remediation tasks. The use of a non-protein tripeptide in the reduction and stabilization of iron ions to obtain magnetic nanoparticles (MNPs) was implemented. The removal of mercury ions in aquatic medium was investigated at different initial values of pH, contact time, temperatures, and parameters of adsorbate-adsorbent. The study of adsorption kinetics was best described using the pseudo-second order velocity equation, and the adsorption equilibrium data best fit the Langmuir equation. Maximum adsorption capacities of 34.48 mg/g were obtained for low mercury concentrations of 1 mg/L at initial conditions and 25°C. Regeneration of the implemented nanoparticles and recovery of Hg^{2+} were demonstrated using 0.1 M KI and HCl up to ten adsorption cycles. From the results obtained, a possibility of application of these nanoparticles for the elimination of mercury in real waters and in large-scale operations is identified.

KEYWORDS: Iron oxide nanoparticles, green synthesis, Glutathione, real water, mercury.

1. INTRODUCTION

Environmental contamination by heavy metals is posing a serious global problem due to its impact on the quality of water resources, food safety and health (Deletic and Wang, 2019; Jing and Kjellerup, 2018). One of these heavy metals is mercury. Although mercury is released into the environment from natural sources, coal-fired power plants and gold mining have been identified as the largest source of mercury (Marimón-Bolívar et al., 2018; Marimon-Bolivar and Toussaint-Jimenez, 2019). For example, 2493.8 tons of mercury were released into the environment from coal combustion between 1978 and 1995. On the other hand, mercury is used in open-pit mining by 15 million miners in over 70 countries in artisanal and small-scale gold mining (Wade, 2013), as it happens in Peru where gold production in Madre de Dios mine was 1583 kilograms of gold in 2016 but that process released an estimated 30–40 tonnes of mercury each year into water (Fraser, 2016). In the case of mercury contamination, in Colombia, anthropic activities related to industry, mining and burning of coal have produced a disturbing increase in the concentration values in bodies of water, air and soil, which are reflected in the loss of quality of life of exposed communities as well as in consumers of contaminated food (Cordy et al., 2015, 2011). The National Water Study (ENA) 2018 estimates a total load discharged to the ground and water of 183 tons in the base year 2016, of which 85% is derived from the gold benefit and 15% from the silver benefit (IDEAM, 2018).

This situation is alarming because mercury does not need to be present in large quantities to generate health risks since it proved to be carcinogenic to mammals due to their capacity of accumulation in organisms, biomagnification through the trophic chains and their resistance to biodegradation (Tang et al., 2016; F. Wang et al., 2016). Methylmercury effects in humans include severe damage to the nervous system, congenital malformations, and even death. These affectations take place because the multiple Hg chemical species have hydrophobic properties and a strong affinity for the biological compounds in the sulfhydryl groups as well as DNA binding. Moreover, conventional techniques for the remediation of heavy metals in water such as chemical precipitation, adsorption, ion exchange, membrane filtration, reverse osmosis, coagulation and flocculation, electrochemical treatment techniques, advanced oxidation processes, and adsorption processes have some disadvantages. Problems such as high energy demand, a large amount of chemical compounds required, production of large volumes of waste, lead to the search for optimization or development of these processes with new materials (Yu et al., 2017).

Within a large number of new materials, Iron Oxide Nanoparticles, especially Magnetite (Fe_3O_4), are shown as a promising alternative for the application in environmental remediation since they have a superparamagnetic behavior. This behavior allows controlling the material in such a way that it minimizes its dispersion to bodies of water and therefore possible contamination(Alvarez et al., 2018; Marimon-Bolívar et al., 2019). However, it is necessary to consider that the production of this material could generate a high environmental impact to ensure responsible application.

For this purpose, green synthesis of magnetic nanoparticles has been studied where plant extracts, marine algae and biomolecules are used as reducing, and stabilizing agents (Liaskovska et al., 2019). With respect to the optimization of magnetic properties necessary for the correct implementation of these materials on a large scale, biomolecules have shown better results. However, these green materials have not been applied for metal removal at levels of concentrations like the levels found in the effluents to establish real adsorption potentials (Fahmy et al., 2018). For these reasons, the adsorption of mercury (II) on magnetic nanoparticles modified with Glutathione (*Glutathione@MNPs*) was studied under different pH values, low concentrations, temperature, and ionic strength conditions. Although there are previous studies (Santos et al., 2016; Xu et al., 2017) where glutathione is used as an agent modifier of magnetic nanoparticles, these studies synthesize the magnetic material through the traditional co-precipitation route and then perform a process of functionality. This way to obtain the magnetic material leads to little feasibility in large scale application due to the environmental impact generated, so that this work allows to use glutathione as a synthesis agent and modifier in a single step which would allow the implementation of this process in environmental remediation tasks.

2. EXPERIMENTAL

2.1. Synthesis of green iron oxide nanoparticles.

Fe_3O_4 NPs obtained through the green method (*Glutathione@MNPs*) were synthesized using a methodology described in a previous work(Marimón-bolívar and González, 2018). Briefly, 10 mL of a $FeCl_3$ (0.1 mol/L) solution was added to a 100-mL beaker under vigorous mechanical stirring at 75°C.Then, 20 mL of an aqueous solution of L-Glutathione (0.214mol/L) was added dropwise into the beaker with the pH value of the mixed solution adjusted to 10. A temperature value of 85°C was reached and it remained in agitation for one hour. Then, the nanoparticles were separated by magnetic field application, washed several times with deionized water and alcohol and dried in vacuum at 40°C for 12 hours.

2.2. Adsorption studies

Glutathione@MNPs obtained by a green route were added at 25°C to aqueous solution of mercury with concentration of 1 ppm prepared from Cl_2Hg standard solution at different pH values (2-10) adjusted with solutions of (0.1M) NaOH or HCl with concentration of nanoparticles of 100 mg/L and a stirring speed of 140 rpm for a standard time of 2 hours. The final concentration of the Hg(II) ions was measured using atomic absorption spectroscopy. The adsorption capacity is calculated on the difference of concentrations at the beginning and the end of the process (Ortiz-Martínez et al., 2016):

$$q_e\left(\frac{mg}{g}\right) = \frac{V(C_0 - C_f)}{m}$$

Where q_e is the adsorption equilibrium of the capacity (mg/g), Co and C_f are the initial concentrations and the equilibrium (mg/l) of the ion in the solution, V is the volume (L) of solution and m is the mass (g) of used adsorbent. Considering the favourable conditions of adsorption tests, kinetics and adsorption isotherms were studied.

2.3. Adsorption kinetics, adsorption isotherm and Adsorption thermodynamics

The adsorption capacity of Hg (II) ions was studied as a function of time. Therefore, an optimal contact time of the adsorption of Hg (II) on the nanoparticles was established and under this equilibrium time condition, the adsorption kinetics was studied. To determine an adequate kinetic model, the adsorption was evaluated in four equations (Supplementary Table 1) (Ali et al., 2018; Robati et al., 2016). To establish parameters for process scaling studies, the enthalpy change (ΔH^0), free energy of Gibbs (ΔG^0) and entropy (ΔS^0) were established by the measurement of the adsorption capacity at different temperatures and the subsequent application of the following equations(Chen et al., 2018):

$$\Delta G^0 = -RT \cdot lnk_L$$
$$lnk_L = \frac{\Delta S^0}{R} - \frac{\Delta H^0}{RT}$$
$$\Delta S^0 = (\Delta H^0 - \Delta G^0)/T$$

2.4. Study of adsorption capacity in real water

For the application in real water, samples from strategic sites in Colombia were selected, specifically in the department of Bolívar and Chocó. The samples were filtered with a 450 mm filter to simulate the water pre-treatment processes that eliminate the suspended material.

3. RESULTS & DISCUSSION

3.1. Characterization of the nanomaterial

The nanoparticles obtained by a green synthesis using Glutathione were characterized to establish the magnetic properties, size, surface chemistry, crystallographic properties, and elemental composition. FTIR analysis showed characteristic peaks of magnetite. The peaks assigned to the iron oxide core can be observed at 580 cm^{-1}

(FeO). Moreover, a low-intensity band was evidenced at 3477 cm^{-1}, which is attributed to amine groups (NH and NH_2), and the peak recognised to the SH group was detected at ~2500 cm^{-1} which is typically very weak. Furthermore, bands were perceived at 2920 cm^{-1}, which is associated to CH sp3 bonds(Marimón-Bolívar et al., 2018; Sadeghi et al., 2016). Instead, it is important to note that the CO stretch band of the carboxyl group, which is representative of the Glutathione spectrum at 1710 cm^{-1}, is absent. This result can be explained by the bonding pattern of the carboxylic acids on the surface of the nanoparticles. Strong adsorption at 1000 cm^{-1} arises from the stretching of the CO single bond. These results revealed that glutathione was attached to the Fe_3O_4 nanoparticles as a carboxylate (Zhang et al., 2006).

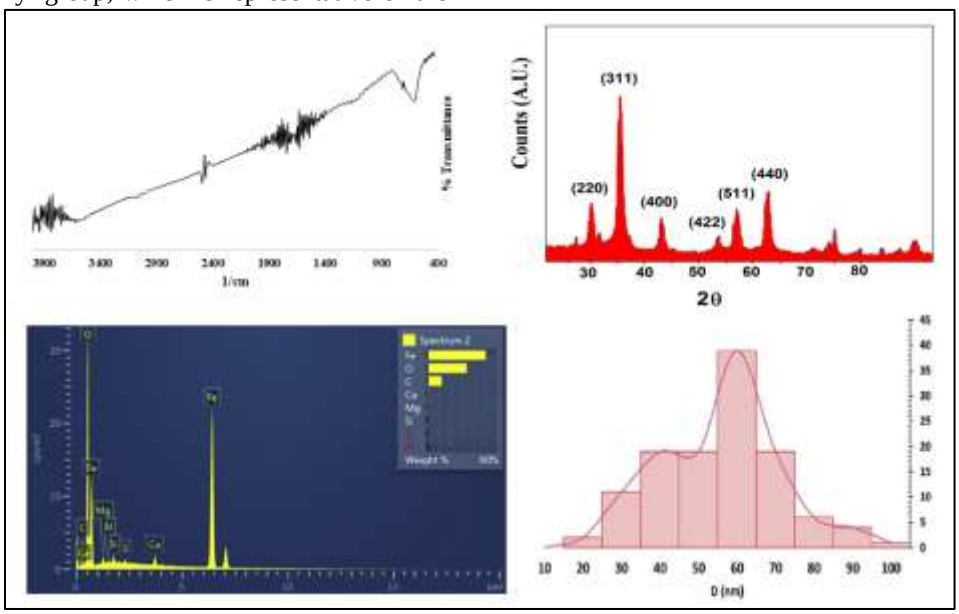

Figure 1. Characterization (FTIR, XRD, EDS, DLS) of Glutathione@MNPs.

XRD characterizations were carried out with CrKα and Cu radiation (1.5406 Å). The angular range was set between 20 and 80° with a scanning speed of 0.04°/s and a step size of 0.04°/s. Fig. 4a and b show the diffractogram of the Glutathione@MNPs. This diffractogram shows indexed peaks as (220), (311), (400), (422), (511) and (440). These peaks correspond to a cubic spinel structure. The crests of XRD were indexed using data from the International Centre for Diffraction Data (ICDD) database. The calculation of the lattice constant yields a value of 8.30 Å which is close to the value for magnetite: 8.39 Å. Furthermore, this structure is recognized for having the peak (311) with the highest intensity.

The EDS spectrum is shown evidence the presence of sulfur, which is part of the thiol groups active on the surface according to the FTIR spectrum. The hydrodynamic size was ~60 nm, while it can be deduced that a greater dispersion in the size of nanoparticles is obtained through green synthesis in comparison to chemical co-precipitation method. Also, this material did not show a reduction in its magnetic properties (Saturation magnetization of 84.5 emu/g) as is usually seen in magnetic nanoparticles obtained by green synthesis, which would make it possible to be used in scale processes (Marimón-bolívar and González, 2018).

3.2. Effect of pH

pH is a significant variable in the behaviour of the compounds in the aqueous medium and therefore for the adsorption process since it affects both the protonation of the functional groups of the surface of the adsorbent nanomaterial and the predominance of the chemical species present in aqueous solution. For this reason, adsorption batch studies were performed in a pH range of 3 to 10 (Figure 2).

The adsorption process is favored when the pH values are close to 7 and 8 (neutral) while in very acidic and basic conditions it was reduced. This occurs because an interaction with protonated mercury ions (Hg^{2+}) takes place when the surface charge of the material is negative (-35mV), as in this case when the pH is close to 7.5 (Marimón-Bolívar and González, 2018). Likewise, in these pH values the functional groups SH-, NH-, NH_2, and COOH- are negatively charged, which favors the electrostatic interactions. Otherwise, in acid pH values, amino and carboxyl groups tend to acquire a neutral or positive charge that gives rise to repulsive forces. For high pH values, the adsorption potential decreases due to the abundance of OH- ions that react with the Hg^{2+} ions to form precipitable compounds, which is not

conducive to the adsorption process(Vikrant and Kim, 2019).

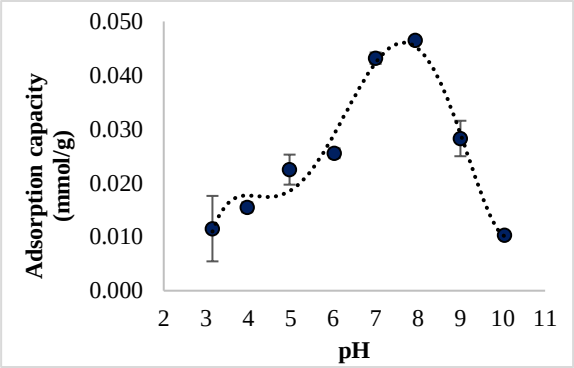

Figure 2. Effect of pH on Hg(II) ions adsorption with *Glutathione@MNPs* (Initial concentration of Hg (II) 1 mg/L; dosage *Glutathione@MNPs* 100 mg/L; T = 25°C; time 60 minutes).

3.3. Adsorption kinetics

Equilibrium time and adsorption kinetic of Hg(II) on *Glutathione@MNPs* were determined. Figure 3 shows how equilibrium time for the adsorption of Hg(II) was reached in 30 minutes approximately since there is no significant difference with adsorption times after 5 hours. This equilibrium time shown is greater than some reported studies (Xiong et al., 2017), which would imply a lower adsorption rate.

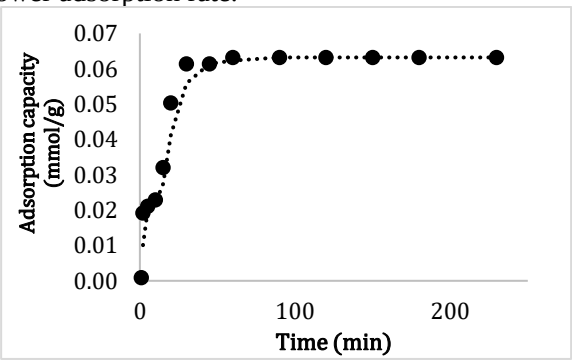

Figure 3. Effect of contact time on the adsorption efficiency of Hg (II). Experimental conditions (1 mg/L Hg, nanoparticle dose 10 mg/L, pH = 8, 140 RPM, 25°C).

However, the experimental conditions are different, since the initial concentrations of the metals used are higher compared to the studies reported, especially in the case of mercury. This difference leads taking more time in the process of reaching the steady state since there is a very high amount of metal in the aqueous medium compared to the concentration of the nanomaterial.

To give clarity to the kinetic phenomenon, an experimental data model with kinetic models (Supplementary Figure 1) in its linear form was established. From the linearized adjustment, it can be observed that the kinetic model that best adapts to the experimental data and that can be used to describe the kinetics of adsorption of Hg (II) on *Glutathione@MNPs* is the Pseudo Second Order model (Supplementary Table 2). This means that the speed at which the interaction between the adsorbate and the adsorbent occurs is dominated by the chemical interactions (chemisorption), which prevail over the transport of adsorbate from the liquid phase to the hydrodynamic layer located around the particle, thus as the transport of this hydrodynamic layer to the surface of the adsorbent (Largitte and Pasquier, 2016).

It should be noticed that the diffusion limiting effects (mass transfer) could also be minimized by the agitation applied to the system so that transport of ions from the liquid to the surface of the material was facilitated. Similarly, Pseudo-second order model describes how adsorption occurs only at localized sites and does not imply an interaction between the adsorbed ions and that the adsorption energy does not depend on the surface coverage, as well as the absorption of metallic ions in the coals activated is governed by a second order rate equation (Moussout et al., 2018). From the above, it can be established interaction of Hg ions with the (-SH) groups on the surface of the nanomaterial are the dominant ones in the process, which would serve as an ideal adsorbent for removal contamination in waters by mercury ions.

3.4. Isothermal studies of the adsorption

Adsorption isotherms describe the equilibrium of the adsorption of a material on a surface at a constant temperature. At high proportions of metal concentration relative to the nanomaterial, the concentration gradient serves as a driving force to overcome the resistance to mass transfer that promotes a favouring of adsorption(Basu et al., 2017). The effect of the nanomaterial dose on the efficiency of heavy metal adsorption was carried out at 20°C with different amounts of *Glutathione@MNPs* (10-100mg/L) using a 50 ml batch with an initial concentration of 1 mg/L of mercury (figure 4). As can be seen, the adsorption capacity of the material decreases with the increase of the adsorbent dose.

This phenomenon happens because when the initial concentration of metal used is high, MNPs with the availability of active functional groups decreases concerning the mercury ions. Conversely, when there is a large amount of MNPs, and the final concentration of the metal is lower, the saturation of the active sites is not

reached and, therefore, a poorer capacity of adsorption is expressed. For example, a 50% decrease in the dose of nanomaterials (from 100 to 50 mg/L) only leads to an increase in the final mercury concentration from 1.8 to 2.9 mmol/L, but the adsorption capacity of 33 increases at 43 mmol/L.

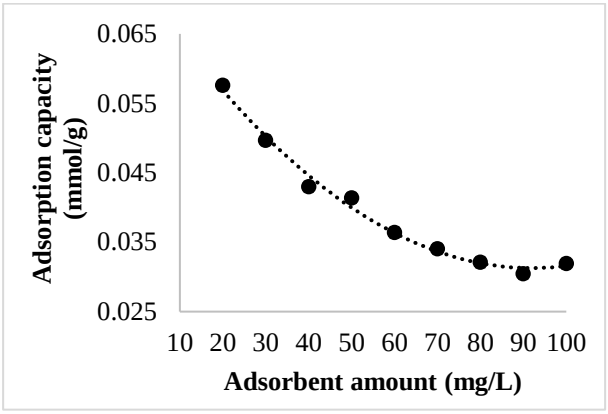

Figure 4. Adsorption isotherm for a) Hg (II)

To determine the adsorption mechanism and the maximum adsorption capacity, the linear adjustments of the isothermal models were made (Supplementary Figure 2). It can be seen that for mercury adsorption, Langmuir equation fits better to the experimental data, which suggests monolayer adsorption on a homogeneous surface. This adsorption is associated with thiol groups, and there is negligible interaction between the species adsorbed (Javier Mancera-rodríguez and Álvarez-león, 2006). These results lead to the fact that, due to the adsorbate/adsorbent interaction, the adsorption energy decreases linearly as the deposition of metal ions increases on the active sites (Tejeda Benitez et al., 2015; Zhao et al., 2016). The parameters resulting from these linear models are shown in Supplementary Table 3.

Here we can notice that all correlation coefficients were higher than 0.92, so that, to a certain extent, the four adsorption isotherm models could be used to describe the Hg(II) adsorption equilibrium, but results would be found more in line with the experimental with Langmuir. From the parameters obtained, it is detected that the maximum adsorption capacity (q_m) of *Glutathione@MNPs* on Hg (II) is 36,126 with a Freundlich coefficient of *1/n* of 0.795 that is less than 1, which expresses an outstanding affinity between the adsorbent and metal. Compared with other studies (Table 1), the adsorption capacity shown by the material is satisfactory since, although it is not one of the highest, the initial concentration of mercury for the studies is lower and this is reflected in the adsorption capacity(Ng et al., 2002).

Table 1. The Maximum adsorption capacity of several adsorbents on Hg (II).

Material	q_m/C_0 *(L/g)*	*Ref*
Dendrimers of polyamidoamine oxide on magnetic graphene	1.16	(Ma et al., 2017)
Chelation fiber functionalized with thiourea	0.20	(Yao et al., 2016)
Modified titanium dioxide nanotubes	0.05	(López-Muñoz et al., 2016)
Chitosan stabilized magnetic iron sulfide nanoparticles	4.42	(M. Sun et al., 2017)
Nano-absorbent PGMA (poly glycidyl methacrylate) magnetic functionalized triethylene teramin	1.08	(Y. Wang et al., 2016)
Exhausted coffee waste	6.35	(Mora Alvarez et al., 2018)
Alkynyl carbon materials	1.61	(Li et al., 2018)
Modified silica gel surface with chelating ligand	1.14	(Lu et al., 2018)
l-Cysteine functionalized bagasse cellulose nanofibers	0.58	(Bansal et al., 2018)
Synthetic FeS and natural pyrite	7.69	(Y. Sun et al., 2017)
Aminophosphonic acid functionalized polyacrylonitrile fiber	3.68	(Xu et al., 2018)
This work	**34.88**	**-**

In other words, for the application in remediation, where mercury contamination values are around 0.1 ppm, working with concentrations higher than 10 ppm gives an erroneous adsorption capacity so, when repeating the studies for the materials compared with contractions equal to the one used in this study, the reported adsorption capacities will be much lower. A proof of this is the capacity of adsorption shown in (Xiong et al., 2017) is 74.85 mg/g being the MOF (Metal Organic Framework) one of the materials with the largest surface

area and hence very high adsorption capacities but with a high environmental impact when this material is obtained.

3.5. Adsorption thermodynamics

The study of adsorption thermodynamics offers more information regarding the viability of the adsorption process and the evaluation of thermodynamic parameters such as the enthalpy energy change (ΔH^0), entropy (ΔS^0), Gibbs free energy (ΔG^0) which are significant parameters for the engineering application of the treatment system (Fosso-Kankeu et al., 2017). For this, adsorption tests were carried out at different temperatures (20-30 °C) as shown in (Supplementary Figure 3). Adsorption capacity was not favoured by the increase in temperature. For the determination of the thermodynamic parameters, the graphs of Ln *K* were made concerning the inverse of the temperatures, where the enthalpy and entropy changes are obtained from the intersection, and the slope of the straight line acquired. These values are shown in Table 2. The positive values of ΔH^0 reveal the endothermic nature of the adsorption process. Likewise, these enthalpy gives indicative of the adsorption mechanisms since it can be used to determine the source of the interaction force that exists between the adsorbent and the adsorbate, indicating the binding strength.

Table 2. Thermodynamic parameters of the adsorption of Hg on *Glutathione@MNPs*

$T\ (K)$	$\Delta G^0 (kJ \cdot mol^{-1})$	$\Delta H^0 (KJ \cdot mol^{-1})$	$\Delta S^0 (KJ \cdot mol^{-1} \cdot K^{-1})$
293	-11.021	45.702	0.118
298	-10.404		
303	-9.828		

Many studies show a decreasing behaviour of the capacity of adsorption when the temperature increases, which leads to ΔH^0 being negative. However, other studies have shown an increase in the ability of adsorption when the temperature increases leading to ΔH^0 being positive (Amer and Awwad, 2018; Miyah et al., 2018). This difference in behaviour is due to the chemical nature of the species that take place in the adsorption. Values of ΔH^0 between 4 and 40 kJ/mol are characteristic of physical interactions, while values of 40 to 800 kJ/mol correspond to chemical interactions (Saman et al., 2017).

The negative ΔG^0 for the adsorption of Hg (II) suggest that this process is spontaneous and favourable. The positive ΔS^0 indicated the increase in randomness during the adsorption or disorder in the solid-liquid interface that is a sample of the dynamic phenomena of desorption adsorption even at equilibrium.

3.6. Adsorption Mechanisms

Based on the previous results (nanomaterial characteristics and the thermodynamic study), the adsorption mechanism of Hg(II) ions on *Glutathione@MNPs* could be established. The process was carried out mainly by ion exchange on the surface of the nanoparticles due to the resulting loads and chemical formations categories of both the metal and the nanomaterial in their dependence on the pH. This formations happens because sulfur is considered to be an electron donor atom that can present complexes with weak metal acids such as mercury (Tran et al., 2015a). Since, a pH close to the neutral values, the mercury species formed ($Hg(OH)_2$, $HgOH^+$ y Hg^{2+}) interacts with the thiol groups in this way:

$$-SH + Hg^{2+} \rightarrow SH - Hg^+$$
$$-SH + HgOH^+ \rightarrow SH - HgOH$$
$$-SH + Hg(OH)_2 \rightarrow -SH \cdots Hg(OH)_2$$
$$-OH + Hg(OH)_2 \rightarrow -O \cdots Hg(OH)_2^{1-} + H^+$$

Because the surface of the nanomaterial is homogeneous (thiols, hydroxyls, amines and carboxyl groups) different adsorption mechanisms take place, giving priority to the route governed by the chemical affinity of the thiols towards mercury ions, but when these are saturated adsorption processes physical in the other ligands take place. The oxygen atoms attached to the hydroxyl groups attached to the iron atoms may also behave as weak bases that interact with the mercury ions.(Tran et al., 2015b):

$$2(-OH) + Hg^{2+} \rightarrow (-O)_2 \cdots HgOH + H^+$$
$$-OH + HgOH^+ \rightarrow -O \cdots HgOH + H^+$$

This proposed mechanism can be supported in the same way by the interpretation of FTIR spectra before and after adsorption (Supplementary Figure 4). There is no remarkable difference in the peaks expressed at ~1628cm^{-1} (carboxyl groups) or 3480cm^{-1} (amino groups) before and after adsorption. For this reason, it is proposed that the active adsorption sites active for the adsorption of mercury would be the -SH groups (Figure 5 and Supplementary Figure 5).

3.7. Desorption and reusability

To evaluate the possibility of regeneration and reusability of the *Glutathione@MNPs* as an adsorbent, batch desorption experiments were conducted. From Figure 6, it can be observed that for the concentrations studied potassium iodide (KI) is the one that best performs the process. This favourability in the process shown by KI is given that the iodine ions have a high affinity for the Hg(II) atoms that cause the phenomenon of saline displacement in comparison with the

dissociation and union of mercury with the Chlorine or hydroxyl ions.

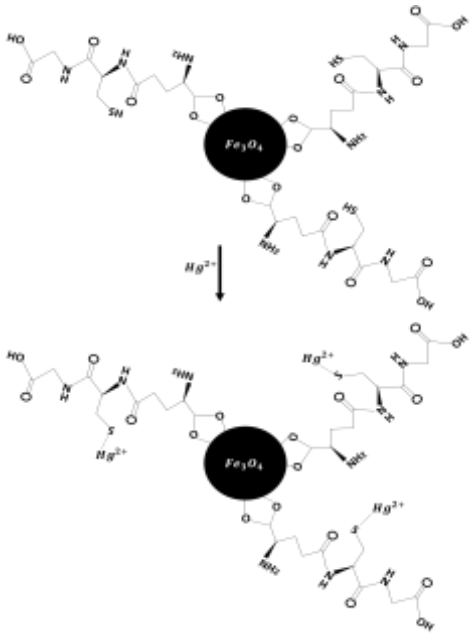

Figure 5. Proposed mechanism adsorption for Hg (II) on *Glutathione@MNPs*.

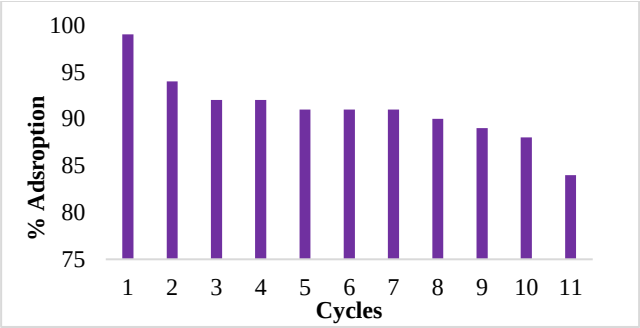

Figure 6. Consecutive adsorption cycles for the adsorption of Hg on *Glutathione@MNPs*.

Reuse tests showed a decrease in the percentage of adsorption higher than 20% only after the tenth cycle of mercury adsorption (Figure 6). These results could be an indicative for the favourability in the application of this material in process at scale.

3.8. Tests with real water

To survey capability of *Glutathione@MNPs* for removal of Hg(II) from real water, some batch experiments were conducted. Concentrations of the initial physicochemical parameters before adsorption were analysed, and the results were summarized in Table 3. It should be noticed that the assessment of the presence of mercury and the best evaluation of the adsorption potential of *Glutathione@MNPs* on mercury ions, made an addition of 100 ppb of the metal before treatment, which is a value 10 times higher than the average of the limits of wastewater discharges allowed by resolution 0631 from Colombia for the different economic sectors(Ministerio de ambiente y desarrollo sostenible (MADS), 2015). The number of nanoparticles added to each treatment was 40 mg/L with an adsorption time of 1 hour at 25°C and a stirring speed of 130rpm.

Table 3. Characteristics of surface and residual water before and after treatment

		Atrato River	Wetland	Quito River	WWTP	San Jorge River
pH		6.30	7.36	5.99	5.32	6.05
Dissolved oxygen (mg/L)		3.4	4.9	6.3	1.5	4.01
DQO (mg/L)		58	45	143	459	50
Conductivity (μS/cm)		272	501	681	747	303
Sulfate (mg/L)		5	11	1	8	6
Nitrates (mg/L)		0.1	0.1	ND	0.3	0.1
Hg (II) (ppb)	Before	1928	1067	1116	984	582
	After	246	153	156	565	78

The results indicated that Hg(II) in real water was removed, and the removal efficiency of Hg(II) reached an average of 78%. It can be observed that in rivers and wetland the percentage of removal is greater than 85% indicating capacity of adsorption. In the case of WWTP, adsorption capacity was not equally favourable (less than 50%), may be due mainly to the physicochemical conditions found, especially the acid character that is lower than the other trials. Likewise, the conductivity value of the sample is higher, which indicates a presence of ions in solution that could interfere in the adsorption process, so an initial pre-treatment of pH adjustment and a decrease of conductivity could increase the efficiency of the process.

These results show that, despite the coexistence of other compounds and non-ideal laboratory characteristics, the function of adsorption of material towards mercury ions is not affected, which would indicate an implementation potential in this type of waters.

CONCLUSIONS

The results obtained confirmed that the material of *Glutathione@MNPs* can eliminate mercury (II) ions from aqueous solutions efficiently. This adsorption

depends strongly on parameters such as initial metal concentration, pH, contact time and coexisting ions.
The adsorption process follows an isotherm behaviour of Langmuir for mercury ions with maximum adsorption capacity on mercury ions of 34.8 mg/g under conditions of mercury concentration of 1 mg/L.

The adsorption kinetics follows a Pseudo-second order regime for mercury with an equilibrium time of less than 30 min. The coexistence of metals from real waters such as magnesium and zinc does not interfere in the removal of mercury. The thermodynamics of the process shows that the interaction with the mercury ions is of chemical order (especially with the functional thiols groups and hydroxyls) since it expresses binding energy of 45.7 kJ/mol.

REFERENCES

Ali, J., Wang, H., Ifthikar, J., Khan, A., Wang, T., Zhan, K., Shahzad, A., Chen, Zhulei, Chen, Zhuqi, 2018. Efficient, stable and selective adsorption of heavy metals by thio-functionalized layered double hydroxide in diverse types of water. Chem. Eng. J. 332, 387–397. https://doi.org/10.1016/j.cej.2017.09.080

Alvarez, P.J.J., Chan, C.K., Elimelech, M., Halas, N.J., Villagrán, D., 2018. Emerging opportunities for nanotechnology to enhance water security. Nat. Nanotechnol. 13, 634–641. https://doi.org/10.1038/s41565-018-0203-2

Amer, M.W., Awwad, A.M., 2018. Removal of As(V) from aqueous solution by adsorption onto nanocrystalline kaolinite: Equilibrium and thermodynamic aspects of adsorption. Environ. Nanotechnology, Monit. Manag. 9, 37–41. https://doi.org/10.1016/j.enmm.2017.12.001

Bansal, M., Ram, B., Chauhan, G.S., Kaushik, A., 2018. L-Cysteine functionalized bagasse cellulose nanofibers for mercury(II) ions adsorption. Int. J. Biol. Macromol. 112, 728–736. https://doi.org/10.1016/j.ijbiomac.2018.01.206

Basu, M., Guha, A.K., Ray, L., 2017. Adsorption of Lead on Cucumber Peel. J. Clean. Prod. 151, 603–615. https://doi.org/10.1016/j.jclepro.2017.03.028

Chen, X., Ye, Q., Ma, D., Chen, J., Wang, Y., Yang, H., Xie, S., Yu, R., Peng, Y., 2018. Gold nanoparticles-pyrrolidinonyl metal phthalocyanine nanoconjugates: Synthesis and photophysical properties. J. Lumin. 195, 348–355. https://doi.org/10.1016/j.jlumin.2017.11.047

Cordy, P., Veiga, M., Bernaudat, L., Garcia, O., 2015. Successful airborne mercury reductions in Colombia. J. Clean. Prod. 108, 992–1001. https://doi.org/10.1016/j.jclepro.2015.06.102

Cordy, P., Veiga, M.M., Salih, I., Al-Saadi, S., Console, S., Garcia, O., Mesa, L.A., Velásquez-López, P.C., Roeser, M., 2011. Mercury contamination from artisanal gold mining in Antioquia, Colombia: The world's highest per capita mercury pollution. Sci. Total Environ. 410, 154–160. https://doi.org/10.1016/j.scitotenv.2011.09.006

Deletic, A., Wang, H., 2019. Water Pollution Control for Sustainable Development. Engineering. https://doi.org/10.1016/J.ENG.2019.07.013

Fahmy, H.M., Mohamed, F.M., Marzouq, M.H., Mustafa, A.B.E.D., Alsoudi, A.M., Ali, O.A., Mohamed, M.A., Mahmoud, F.A., 2018. Review of Green Methods of Iron Nanoparticles Synthesis and Applications. Bionanoscience. https://doi.org/10.1007/s12668-018-0516-5

Fosso-Kankeu, E., Mittal, H., Waanders, F., Ray, S.S., 2017. Thermodynamic properties and adsorption behaviour of hydrogel nanocomposites for cadmium removal from mine effluents. J. Ind. Eng. Chem. 48, 151–161. https://doi.org/10.1016/j.jiec.2016.12.033

Fraser, B., 2016. Peru's gold rush raises health fears. Nature. https://doi.org/10.1038/nature.2016.19999

IDEAM, 2018. Estudio Nacional del Agua 2018.

Javier Mancera-rodríguez, N., Álvarez-león, R., 2006. Current State of Knowledge of the Concentration of Mercury and Other Heavy Metals in Fresh Water Fish in Colombia. Acta Biológica Colomb. 11, 3–23.

Jing, R., Kjellerup, B. V., 2018. Biogeochemical cycling of metals impacting by microbial mobilization and immobilization. J. Environ. Sci. (China). https://doi.org/10.1016/j.jes.2017.04.035

Largitte, L., Pasquier, R., 2016. A review of the kinetics adsorption models and their application to the adsorption of lead by an activated carbon. Chem. Eng. Res. Des. 109, 495–504. https://doi.org/10.1016/j.cherd.2016.02.006

Li, Y., Li, W., Liu, Q., Meng, H., Lu, Y., Li, C., 2018. Alkynyl carbon materials as novel and efficient sorbents for the adsorption of mercury(II) from wastewater. J. Environ. Sci. (China) 68, 169–176. https://doi.org/10.1016/j.jes.2016.12.016

Liaskovska, M., Tatarchuk, T., Bououdina, M., Mironyuk, I., 2019. Green Synthesis of Magnetic Spinel Nanoparticles. Springer, Cham, pp. 389–398. https://doi.org/10.1007/978-3-030-17755-3_25

López-Muñoz, M.J., Arencibia, A., Cerro, L., Pascual, R., Melgar, Á., 2016. Adsorption of Hg(II) from aqueous solutions using TiO2 and titanate nanotube adsorbents. Appl. Surf. Sci. 367, 91–100. https://doi.org/10.1016/j.apsusc.2016.01.109

Lu, J., Wu, X., Li, Y., Cui, W., Liang, Y., 2018. Modified silica gel surface with chelating ligand for effective mercury ions adsorption. Surfaces and Interfaces 12, 108–115. https://doi.org/10.1016/j.surfin.2018.04.005

Ma, Y.X., Xing, D., Shao, W.J., Du, X.Y., La, P.Q., 2017. Preparation of polyamidoamine dendrimers functionalized magnetic graphene oxide for the adsorption of Hg(II) in aqueous solution. J. Colloid Interface Sci. 505, 352–363. https://doi.org/10.1016/j.jcis.2017.05.104

Marimón-bolívar, W., González, E.E., 2018. Study of agglomeration and magnetic sedimentation of Glutathione@Fe3O4 nanoparticles in water medium. DYNA 85, 19–26. https://doi.org/10.15446/dyna.v85n205.68245

Marimón-Bolívar, W., González, E.E., 2018. Green synthesis with enhanced magnetization and life cycle assessment of Fe3O4 nanoparticles. Environ. Nanotechnology, Monit. Manag. 9, 58–66. https://doi.org/10.1016/j.enmm.2017.12.003

Marimón-Bolívar, W., Tejeda-Benítez, L., Herrera, A.P., 2018. Removal of mercury (II) from water using magnetic nanoparticles coated with amino organic ligands and yam peel biomass. Environ. Nanotechnology, Monit. Manag. https://doi.org/10.1016/j.enmm.2018.10.001

Marimon-Bolívar, W., Tejeda-Benítez, L.P., Núñez-Avilés, C.A., De Léon-Pérez, D. De, 2019. Evaluation of the in vivo toxicity of green magnetic nanoparticles using Caenorhabditis elegans as a biological model. Environ. Nanotechnology, Monit. Manag. 12, 100253. https://doi.org/10.1016/J.ENMM.2019.100253

Marimon-Bolivar, W., Toussaint-Jimenez, N., 2019. A review on green synthesis of magnetic nanoparticles (magnetite) for environmental applications, in: 2019 Congreso Internacional de Innovacion y Tendencias En Ingenieria, CONIITI 2019 - Conference Proceedings. Institute of Electrical and Electronics Engineers Inc. https://doi.org/10.1109/CONIITI48476.2019.8960849

Ministerio de ambiente y desarrollo sostenible (MADS), 2015. Resolución N° 1312.

Miyah, Y., Lahrichi, A., Idrissi, M., Khalil, A., Zerrouq, F., 2018. Adsorption of methylene blue dye from aqueous solutions onto walnut shells powder: Equilibrium and kinetic studies. Surfaces and Interfaces 11, 74–81. https://doi.org/10.1016/j.surfin.2018.03.006

Mora Alvarez, N.M., Pastrana, J.M., Lagos, Y., Lozada, J.J., 2018. Evaluation of mercury (Hg2+) adsorption capacity using exhausted coffee waste. Sustain. Chem. Pharm. 10, 60–70. https://doi.org/10.1016/j.scp.2018.09.004

Moussout, H., Ahlafi, H., Aazza, M., Maghat, H., 2018. Critical of linear and nonlinear equations of pseudo-first order and pseudo-second order kinetic models. Karbala Int. J. Mod. Sci. 4, 244–254. https://doi.org/10.1016/j.kijoms.2018.04.001

Ng, C., Losso, J.N., Marshall, W.E., Rao, R.M., 2002. Freundlich adsorption isotherms of agricultural by-product-based powdered activated carbons in a geosmin-water system. Bioresour. Technol. 85, 131–135. https://doi.org/10.1016/S0960-8524(02)00093-7

Ortiz-Martínez, K., Reddy, P., Cabrera-Lafaurie, W.A., Román, F.R., Hernández-Maldonado, A.J., 2016. Single and multi-component adsorptive removal of bisphenol A and 2,4-dichlorophenol from aqueous solutions with transition metal modified inorganic-organic pillared clay composites: Effect of pH and presence of humic acid. J. Hazard. Mater. 312, 262–271. https://doi.org/10.1016/j.jhazmat.2016.03.073

Robati, D., Mirza, B., Rajabi, M., Moradi, O., Tyagi, I., Agarwal, S., Gupta, V.K., 2016. Removal of hazardous dyes-BR 12 and methyl orange using graphene oxide as an adsorbent from aqueous phase. Chem. Eng. J. 284, 687–697. https://doi.org/10.1016/j.cej.2015.08.131

Sadeghi, M., Hanifpour, F., Taheri, R., Javadian, H., Ghasemi, M., 2016. Comparison of using formaldehyde and carboxy methyl chitosan in preparation of Fe3O4superparamagnetic nanoparticles-chitosan hydrogel network: Sorption behavior toward bovine serum albumin. Process Saf. Environ. Prot. 102, 119–128. https://doi.org/10.1016/j.psep.2016.03.005

Saman, N., Johari, K., Song, S.T., Kong, H., Cheu, S.C., Mat, H., 2017. High removal efficacy of Hg(II) and MeHg(II) ions from aqueous solution by organoalkoxysilane-grafted lignocellulosic waste biomass. Chemosphere 171, 19–30. https://doi.org/10.1016/j.chemosphere.2016.12.049

Santos, M.C., Seabra, A.B., Pelegrino, M.T., Haddad, P.S., 2016. Synthesis, characterization and cytotoxicity of glutathione- and PEG-glutathione-superparamagnetic iron oxide nanoparticles for nitric oxide delivery. Appl. Surf. Sci. 367, 26–35. https://doi.org/10.1016/j.apsusc.2016.01.039

Sun, M., Cheng, G., Ge, X., Chen, M., Wang, C., Lou, L., Xu, X., 2017. Aqueous Hg(II) immobilization by chitosan stabilized magnetic iron sulfide nanoparticles. Sci. Total Environ. 621, 1074–1083. https://doi.org/10.1016/j.scitotenv.2017.10.119

Sun, Y., Lv, D., Zhou, J., Zhou, X., Lou, Z., Baig, S.A., Xu, X., 2017. Adsorption of mercury (II) from aqueous solutions using FeS and pyrite: A comparative study. Chemosphere 185, 452–461. https://doi.org/10.1016/j.chemosphere.2017.07.047

Tang, W., Duan, S., Shan, B., Zhang, H., Zhang, W., Zhao, Y., Zhang, C., 2016. Concentrations, diffusive fluxes and toxicity of heavy metals in pore water of the Fuyang River, Haihe Basin. Ecotoxicol. Environ. Saf. 127, 80–6. https://doi.org/10.1016/j.ecoenv.2016.01.013

Tejeda Benitez, L., Marimón Bolivar, W., Tejada Tovar, C., Quiñones Bolaños, E., 2015. Absorción de Cromo Hexavalente en soluciones acuosas por cascaras de naranja (Citrus sinensis). Prod. más Limpia 10, 9–21.

Tran, L., Wu, P., Zhu, Y., Liu, S., Zhu, N., 2015a. Comparative study of Hg(II) adsorption by thiol- and hydroxyl-containing bifunctional montmorillonite and vermiculite. Appl. Surf. Sci. 356, 91–101. https://doi.org/10.1016/j.apsusc.2015.08.038

Tran, L., Wu, P., Zhu, Y., Liu, S., Zhu, N., 2015b. Comparative study of Hg(II) adsorption by thiol- and hydroxyl-containing bifunctional montmorillonite and vermiculite. Appl. Surf. Sci. 356, 91–101. https://doi.org/10.1016/j.apsusc.2015.08.038

Vikrant, K., Kim, K.-H., 2019. Nanomaterials for the adsorptive treatment of Hg(II) ions from water. Chem. Eng. J. 358, 264–282. https://doi.org/10.1016/j.cej.2018.10.022

Wade, L., 2013. Gold's dark side. Science (80-.). https://doi.org/10.1126/science.341.6153.1448

Wang, F., Lu, X., Li, X., 2016. Selective removals of heavy metals (Pb2+, Cu2+, and Cd2+) from wastewater by gelation with alginate for effective metal recovery. J. Hazard. Mater. 308, 75–83. https://doi.org/10.1016/j.jhazmat.2016.01.021

Wang, Y., Zhang, Y., Hou, C., He, X., Liu, M., 2016. Preparation of a novel TETA functionalized magnetic PGMA nano-absorbent by ATRP method and used for highly effective adsorption of Hg(II). J. Taiwan Inst. Chem. Eng. 58, 283–289. https://doi.org/10.1016/j.jtice.2015.05.044

Xiong, Y.Y., Li, J.Q., Gong, L. Le, Feng, X.F., Meng, L.N., Zhang, L., Meng, P.P., Luo, M.B., Luo, F., 2017. Using MOF-74 for Hg2+ removal from ultra-low concentration aqueous solution. J. Solid State Chem. 246, 16–22. https://doi.org/10.1016/j.jssc.2016.10.018

Xu, G., Wang, L., Xie, Y., Tao, M., Zhang, W., 2018. Highly selective and efficient adsorption of Hg2+by a recyclable aminophosphonic acid functionalized polyacrylonitrile fiber. J. Hazard. Mater. 344, 679–688. https://doi.org/10.1016/j.jhazmat.2017.11.017

Xu, P., Zeng, G.M., Huang, D.L., Yan, M., Chen, M., Lai, C., Jiang, H., Wu, H.P., Chen, G.M., Wan, J., 2017. Fabrication of reduced glutathione functionalized iron oxide nanoparticles for magnetic removal of Pb(II) from wastewater. J. Taiwan Inst. Chem. Eng. 71, 165–173. https://doi.org/10.1016/J.JTICE.2016.11.031

Yao, X., Wang, H., Ma, Z., Liu, M., Zhao, X., Jia, D., 2016. Adsorption of Hg(II) from aqueous solution using thiourea functionalized chelating fiber. Chinese J. Chem. Eng. 24, 1344–1352. https://doi.org/10.1016/j.cjche.2016.07.008

Yu, X., Xin, P., Lu, C., Robinson, C., Li, L., Barry, D.A., 2017. Effects of episodic rainfall on a subterranean estuary. Water Resour. Res. 53, 5774–5787. https://doi.org/10.1002/2017WR020809

Zhang, L., He, R., Gu, H.-C., 2006. Oleic acid coating on the monodisperse magnetite nanoparticles. Appl. Surf. Sci. 253, 2611–2617. https://doi.org/10.1016/j.apsusc.2006.05.023

Zhao, J., Liu, J., Li, N., Wang, W., Nan, J., Zhao, Z., Cui, F., 2016. Highly efficient removal of bivalent heavy metals from aqueous systems by magnetic porous Fe3O4-MnO2: Adsorption behavior and process study. Chem. Eng. J. 304, 737–746. https://doi.org/10.1016/j.cej.2016.07.003